

## RESEARCH ARTICLE

10.1002/2016JD024871

## Key Points:

- Elevation-dependent warming is present within an initially relatively low elevation range but is absent when elevation continues to raise
- Elevation-dependent warming can expand to higher elevations when more serious warming occurs in the future
- Snow-albedo feedback is mostly responsible for the future elevation-dependent warming on the Tibetan Plateau

## Correspondence to:

D. Guo,  
guodl@mail.iap.ac.cn

## Citation:

Guo, D., E. Yu, and H. Wang (2016), Will the Tibetan Plateau warming depend on elevation in the future?, *J. Geophys. Res. Atmos.*, 121, 3969–3978, doi:10.1002/2016JD024871.

Received 28 JAN 2016

Accepted 26 MAR 2016

Accepted article online 6 APR 2016

Published online 29 APR 2016

## Will the Tibetan Plateau warming depend on elevation in the future?

Donglin Guo<sup>1,2,3</sup>, Entao Yu<sup>1,2</sup>, and Huijun Wang<sup>4,1</sup>

<sup>1</sup>Nansen-Zhu International Research Center, Institute of Atmospheric Physics, Chinese Academy of Sciences, Beijing, China, <sup>2</sup>Collaborative Innovation Center on Forecast and Evaluation of Meteorological Disasters (CIC-FEMD), Nanjing University of Information Science and Technology, Nanjing, China, <sup>3</sup>Climate Change Research Center, Chinese Academy of Sciences, Beijing, China, <sup>4</sup>Key Laboratory of Meteorological Disaster, Ministry of Education/Joint International Research Laboratory of Climate and Environment Change/Collaborative Innovation Center on Forecast and Evaluation of Meteorological Disasters (CIC-FEMD), Nanjing University of Information Science and Technology, Nanjing, China

**Abstract** Elevation-dependent warming, greater warming at higher elevations, tends to accelerate the ablation of solid water reserves on the Tibetan Plateau and is thus expected to affect the sustainable water supply of the plateau. In the context of a global climate that is predicted to continue to warm, whether elevation-dependent warming exists on the Tibetan Plateau in the future and, if so, what its characteristics and mechanisms are, are important issues that have not yet been fully assessed. Using six sets of high-resolution outputs from dynamical downscaling simulations based on regional climate models, we investigated the future situation regarding the elevation dependency of climate warming on the Tibetan Plateau. The simulated air temperature trends from the six simulations are validated using meteorological station observations. The trends from only two simulations are selected for analysis due to their statistically significant correlation with the observations. The warming rate first increases to a peak and then slightly declines along with elevation increasing from 2000 m to 5600 m. The peak of the warming rate is reached at variable elevations (4400–5200 m), which depends on the intensity of the warming. The elevation at which this peak occurs increases when the warming intensifies. Such elevation-dependent warming is mostly caused by the decrease in upward short-wave radiation due to the depletion of snow based on surface energy budget analysis. These results provide some understanding of the future elevation-dependent warming on the Tibetan Plateau, which will be useful for evaluating the sustainability of water resources of the Tibetan Plateau water-affected area.

### 1. Introduction

With an average height of more than 4000 m and an area of approximately  $2.5 \times 10^6 \text{ km}^2$ , the Tibetan Plateau is the highest and the most extensive highland in the world and has been nicknamed the “third pole” of the Earth [Qiu, 2008]. In China, the Tibetan Plateau is also recognized as the “Asian water tower” because glaciers (approximately  $1.0 \times 10^5 \text{ km}^2$  [Yao *et al.*, 2012]), snow (approximately  $41.9 \times 10^9 \text{ m}^3 \text{ yr}^{-1}$  water equivalent [Li *et al.*, 2008]), and permafrost (approximately  $1.5 \times 10^6 \text{ km}^2$  [Li and Cheng, 1996; Guo and Wang, 2013]) are extensively present on the Tibetan Plateau. These solid water resources feed the major rivers in Southeast Asia, including the Indus, Ganges, Brahmaputra, Mekong, Yangtze, and Yellow Rivers, which provide water to more than 1.4 billion people (more than 20% of the global population) [Immerzeel *et al.*, 2010; Yao *et al.*, 2012].

Nevertheless, these solid water reserves are mostly distributed in higher-elevation areas with colder climate conditions on the Tibetan Plateau. A significant climate warming has been observed on the Tibetan Plateau in recent decades [Liu and Chen, 2000; Guo and Wang, 2012; Yang *et al.*, 2010; Zhou *et al.*, 2016]. For example, an average warming of  $1.3^\circ\text{C}$  occurred on the Tibetan Plateau from 1961 to 2007 [Guo and Wang, 2012]. An elevation-dependent warming law, greater warming rates at higher elevations, has been observed on the Tibetan Plateau [Liu and Chen, 2000; Qin *et al.*, 2009; Rangwala *et al.*, 2010]. This law tends to accelerate the ablation of the solid water reserves because of their distributions at higher elevations and is thus expected to affect the sustainable water supply of the Tibetan Plateau to the downstream areas [Immerzeel *et al.*, 2010; Qin *et al.*, 2014; Pepin *et al.*, 2015].

The Tibetan Plateau climate is predicted to continue to warm more seriously in the next 100 years [Guo *et al.*, 2012; Su *et al.*, 2013; Zhou *et al.*, 2014; Zhang *et al.*, 2015; Hu *et al.*, 2015]. Hu *et al.* [2015] showed that an

average warming of 2.7°C will occur on the Tibetan Plateau during 2081–2100 relative to 1986–2005 in the Representative Concentration Pathway (RCP) 4.5 scenario [Hu et al., 2015; Zhang et al., 2015]. The warming is more significant relative to nonmountain regions at the same latitude [Rangwala et al., 2013] and is 1.5 times higher than the global mean level of 1.8°C in the same RCP scenario [Intergovernmental Panel on Climate Change, 2013]. If the elevation dependency law continues in the future warming, the people in the Tibetan Plateau water-affected areas will face a water scarcity crisis. Therefore, studying the future elevation dependency of climate warming on the Tibetan Plateau is important for evaluating the sustainability of the water supply of the Tibetan Plateau and the associated development of appropriate water policies for the downstream countries.

Because of growing concerns about these important implications, research efforts have concentrated on investigating elevation-dependent warming and the mechanisms on the Tibetan Plateau [Liu and Chen, 2000; You et al., 2008; Qin et al., 2009; Liu et al., 2009; Rangwala et al., 2010; Rangwala and Miller, 2012; Yang et al., 2014; Pepin et al., 2015]. Using monthly surface air temperature data from meteorological stations, Liu and Chen [2000] found that significant warming has occurred on the Tibetan Plateau since the mid-1950s, with an average warming rate of 0.16°C decade<sup>-1</sup> from 1955 to 1996. Furthermore, the warming rates increase with rising elevations. With an offset of weakness in the station observation studies due to sparse observation stations in the western Tibetan Plateau, the Moderate Resolution Imaging Spectroradiometer (MODIS)-derived land surface temperature was used to explore the elevation-dependent warming on the Tibetan Plateau [Qin et al., 2009]. The results show that the warming rate first increases with elevation rising from 3000 to 4800 m and then becomes stable, with a slight decline near the highest elevations. Numerical simulation was also used to reproduce the elevation dependency of climate warming from 1961 to 1990 on the Tibetan Plateau [Rangwala et al., 2010]. Furthermore, elevation-dependent increase in downward long-wave radiation influenced by surface specific humidity and absorbed solar radiation influenced by snow cover and atmospheric aerosols are responsible for the elevation-dependent warming [Rangwala et al., 2010].

These studies mentioned above provide key insights into the elevation dependency of climate warming and the mechanisms on the Tibetan Plateau during the recent decades. Nevertheless, the future elevation-dependent warming on the Tibetan Plateau has not been fully assessed. Although Rangwala et al. [2010] referred to a projection with respect to the Tibetan Plateau warming's relationship with elevation from 1960 to 2100 based on the output from Goddard Institute for Space Studies Atmosphere-Ocean Model (GISS-AOM), the results are less detailed due to the coarse model resolution of 3° longitude × 4° latitude.

The objectives of the present study are to assess the future elevation-dependent warming situation and mechanisms on the Tibetan Plateau using the high-resolution outputs from multiple dynamical downscaling simulations. A validation of the simulation results is performed based on meteorological station observations before assessing. The data and methods are described in section 2. The results and discussion are presented in section 3, followed by a summary of the key findings of this study in section 4.

## 2. Model, Data, and Methods

The four data sets from dynamical downscaling simulations are obtained from the Coordinated Regional Climate Downscaling Experiment (CORDEX) in East Asia [Giorgi et al., 2009]. They include the data archived from Hadley Centre Global Environmental Model version 3 regional climate model (HadGEM3-RA) [Martin et al., 2006], regional climate model version 4 (RegCM4) [Giorgi et al., 2012], mesoscale model version 5 (MM5) [Lee et al., 2004], and Weather Research and Forecasting version 3.2 (WRF3.2) [Skamarock et al., 2008] nested within the same model of the Hadley Centre Global Environment Model version 2 Atmosphere-Ocean (HadGEM2-AO) Model [Baek et al., 2013], which are named as HadGEM2-AO/HadGEM3-RA, HadGEM2-AO/RegCM4, HadGEM2-AO/MM5, and HadGEM2-AO/WRF, respectively (Table 1). All four simulations have similar model domains, including East Asia, India, the western Pacific Ocean, and the northern part of Australia and the same horizontal resolution of 50 km following the protocol of the CORDEX for Asia [Giorgi et al., 2009]. The HadGEM2-AO/HadGEM3-RA simulation is conducted from 1950 to 2100, which includes the historical simulation (1950–2005) and the future simulation (2006–2100) under the RCP4.5 and RCP8.5 scenarios. The HadGEM2-AO/RegCM4 simulation is conducted from 1979 to 2049, including the historical simulation (1979–2005) and the future simulation

**Table 1.** Details of Six Dynamical Downscaling Simulations

Model Name	Horizontal Resolution	Model Domain	Historical Simulation Period	Future Simulation Period	Scenario
HadGEM2-AO/HadGEM3-RA	50 km	CORDEX-East Asia domain	1950–2005	2006–2100	RCP 4.5 and RCP 8.5
HadGEM2-AO/RegCM4	50 km	CORDEX-East Asia domain	1979–2005	2006–2050	RCP 4.5 and RCP 8.5
HadGEM2-AO/MM5	50 km	CORDEX-East Asia domain	1979–2005	2006–2049	RCP 4.5 and RCP 8.5
HadGEM2-AO/WRF	50 km	CORDEX-East Asia domain	1979–2005	2006–2049	RCP 4.5 and RCP 8.5
BCC-CSM1.1/RegCM4	50 km	160 (west-east) × 109 (north-south) grids, centering at 35°N, 105°E	1950–2005	2006–2099	RCP 4.5 and RCP 8.5
MIROC5/WRF	30 km	255 (west-east) × 205 (north-south) grids, centering at 35°N, 103°E	1946–2005	2006–2100	RCP 6.0

(2006–2050) under the RCP4.5 and RCP8.5 scenarios, and the HadGEM2-AO/MM5 and HadGEM2-AO/WRF simulations are conducted from 1979 to 2049, including the historical simulation (1979–2005) and the future simulation (2006–2049) under the RCP4.5 and RCP8.5 scenarios. The physical schemes and more details regarding each simulation can be found at the website (<https://cordex-ea.climate.go.kr/main/mainPage.do>).

One data set is archived from RegCM4 nested within Beijing Climate Center Climate System Model version 1.1 (BCC-CSM1.1) [Wu *et al.*, 2010], which is named as BCC-CSM1.1/RegCM4 (Table 1). The period of simulation is from 1950 to 2099 (the first year is considered as the spin-up period), with the historical simulation of 1950–2005 and the future simulation of 2006–2099 under the RCP4.5 and RCP8.5 scenarios. The model domain covers 160 grids (west-east) × 109 grids (north-south), with the center at (35°N, 105°E), with horizontal and vertical resolutions of 50 km and 18 sigma layers from the surface up to a model top at 10 hPa. The physical schemes and additional details can be found in the works of Gao *et al.* [2013], Ji and Kang [2013], and Yu and Xiang [2015].

One data set is archived from WRF3.4 driven by the initial and boundary conditions from Model for Interdisciplinary Research on Climate version 5 (MIROC5) [Watanabe *et al.*, 2010] and is named MIROC5/WRF (Table 1). The microphysics is the Single-Moment 6-Class Microphysics scheme [Hong and Lim, 2006]. The radiation transfer scheme is calculated by Community Atmosphere Model version 3.0 [Collins *et al.*, 2004]. The cumulus convective precipitation is the Kain-Fritsch scheme [Kain, 2004], and the planetary boundary layer is the Yonsei University scheme [Hong *et al.*, 2006]. The land surface model employs the Noah land surface model [Niu *et al.*, 2011]. The simulation was conducted from 1946 to 2100, and the first year of the period was taken as the spin-up period. The historical simulation is from 1946 to 2005, and the future simulation is from 2006 to 2100 under the RCP6.0 scenario. The horizontal resolution of the simulation is 30 km, with 35 vertical sigma layers. The model domain covers 255 grids (west-east) × 205 grids (north-south), with the center at (35°N, 103°E). More detailed information can be found in Yu *et al.* [2014]. Notably, because this study focuses on yearly climate warming's relationship with elevation, the annual mean data sets from these simulations are used.

Meteorological stations that observed yearly surface air temperatures are provided by the China Meteorological Administration and are used to validate the model simulations. Stations with elevation above 2000 m are selected, and they cover a total elevation range from 2032 m to 4700 m. These stations are mostly distributed at the central and eastern Tibetan Plateau (Figure 1). The data period is from 1961 to 2007. Data quality control is based on a basic logic test and a spatial consistency test. In addition, the multiple analyses of series for homogenization method [Li and Yan, 2009] and the Easterling-Peterson techniques are used to assess the homogeneity of the data [Easterling and Peterson, 1995; Li *et al.*, 2004]. These data are reliable and have been widely used to study climate change during the past decades [You *et al.*, 2008; Wang and Sun, 2009; Guo and Wang, 2012; Wang *et al.*, 2012; Guo and Wang, 2014; Wu *et al.*, 2015].

The surface elevation data used are the global digital elevation data, GTOPO30, which are developed by the U.S. Geological Survey's Center for Earth Resources Observation and Science (<http://eros.usgs.gov/>, 12 January 2016). The data have a horizontal resolution of approximately 1 km. In addition, together with all six sets of simulation data, the surface elevation data were interpolated into the horizontal resolution of 30 km of the MIROC5/WRF simulation for homogenous comparison. The trends of various variables are computed as the slope of the linear fit derived by ordinary least squares regression.

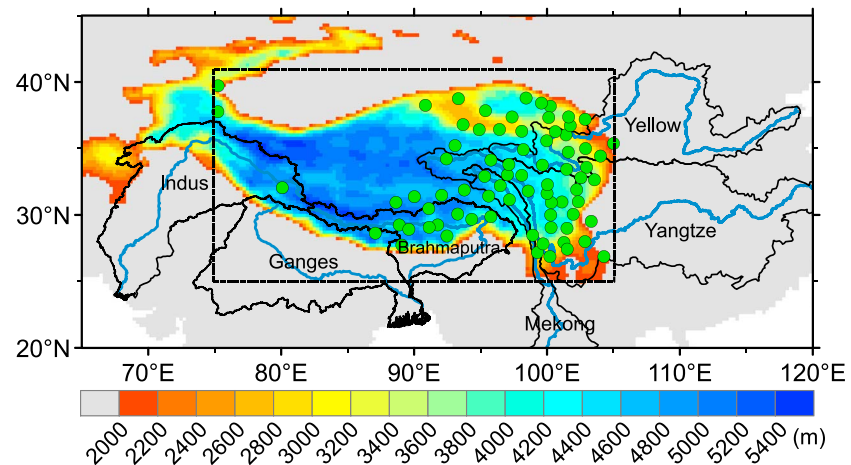


**Figure 1.** Location of the study area (75–105°E, 25–41°N; shown as black rectangle), the related basin boundaries and river courses (Indus, Ganges, Brahmaputra, Mekong, Yangtze, and Yellow Rivers; based on a data set (<http://freegisdata.rtwilson.com/>), 12 January 2016) in Southeast Asian, and meteorological observation stations (green dots).

### 3. Results and Discussion

#### 3.1. Validation of the Model

A validation of the dynamical downscaling simulations is first performed using station observations before they are used for the analysis. As shown in Figure 2, different simulations present large differences in agreement levels between simulated and observed trends from 1979 to 2005—the longest period shared by all six simulations. The correlation coefficients between simulations and observations range from  $-0.30$  to  $0.83$  among the six dynamical downscaling simulations. Relative to the corresponding global circulation models (GCMs), the simulated results have been improved using dynamical downscaling method. For example, the correlation coefficient between simulated and observed trends becomes  $0.41$  (HadGEM2-AO/RegCM4) from original  $0.04$  (HadGEM2-AO). But, bias still exists (Figure 2). The simulation that presents the best correlation is HadGEM2-AO/RegCM4, and the simulation that presents the worst correlation is HadGEM2-AO/HadGEM3-RA. Simulations with higher correlation coefficients show more clearly the elevation-dependent warming that is displayed in the station observations. Notably, in the validation of HadGEM2-AO/RegCM4 (Figure 2f), there is a mark (blue 7) that has large trend but relatively low elevation, which is true for both simulated and observed results. The mark is generated by regional particularities. Major stations included in the mark are located in the northern Tibetan Plateau, where the warming violates the law of elevation-dependent warming on the Tibetan Plateau [Guo and Wang, 2012].

The disagreement in the simulated and observed results is partially derived from the corresponding GCM simulations that provide the driving data (not shown). In addition, model domain, physical schemes, and less accurate surface data used in the simulations may be responsible for the disagreement [Qu *et al.*, 2009; Gao *et al.*, 2013; Han *et al.*, 2015; Guo and Wang, 2016]. The simulated results are more reasonable when only the Tibetan Plateau region is selected as model domain instead of China and its adjacent regions [Qu *et al.*, 2009]. When a set of land cover data that include more observations was used, Han *et al.* [2015] found that the simulated bias in air temperature reduced on the Tibetan Plateau. Besides, scale mismatch in the comparisons could be one of the sources that result in the disagreement. The comparisons are based on grid-mean simulated results and individual station observations. An individual site may not fully represent the situation in a grid area of  $30 \times 30$  km [Lawrence *et al.*, 2012; Guo and Wang, 2013]. This could be particularly significant on the Tibetan Plateau, where the topography is very rugged and varied.

Despite these reasons, a statistical significance level of above 95% for the correlation coefficient is considered as a criterion to select the “reliable” simulations for future analysis. The statistical significance is assessed using the Student’s *t* test method, with a degree of freedom of 12 [ $14$  (sample number)  $- 2$ ]. Accordingly, only the HadGEM2-AO/RegCM4 and MIROC5/WRF simulations are appropriate, which suggests that a larger proportion of dynamical downscaling simulations cannot be directly used to study climate warming’s relationship with elevation on the Tibetan Plateau, and validation with respect to model performance is necessary.

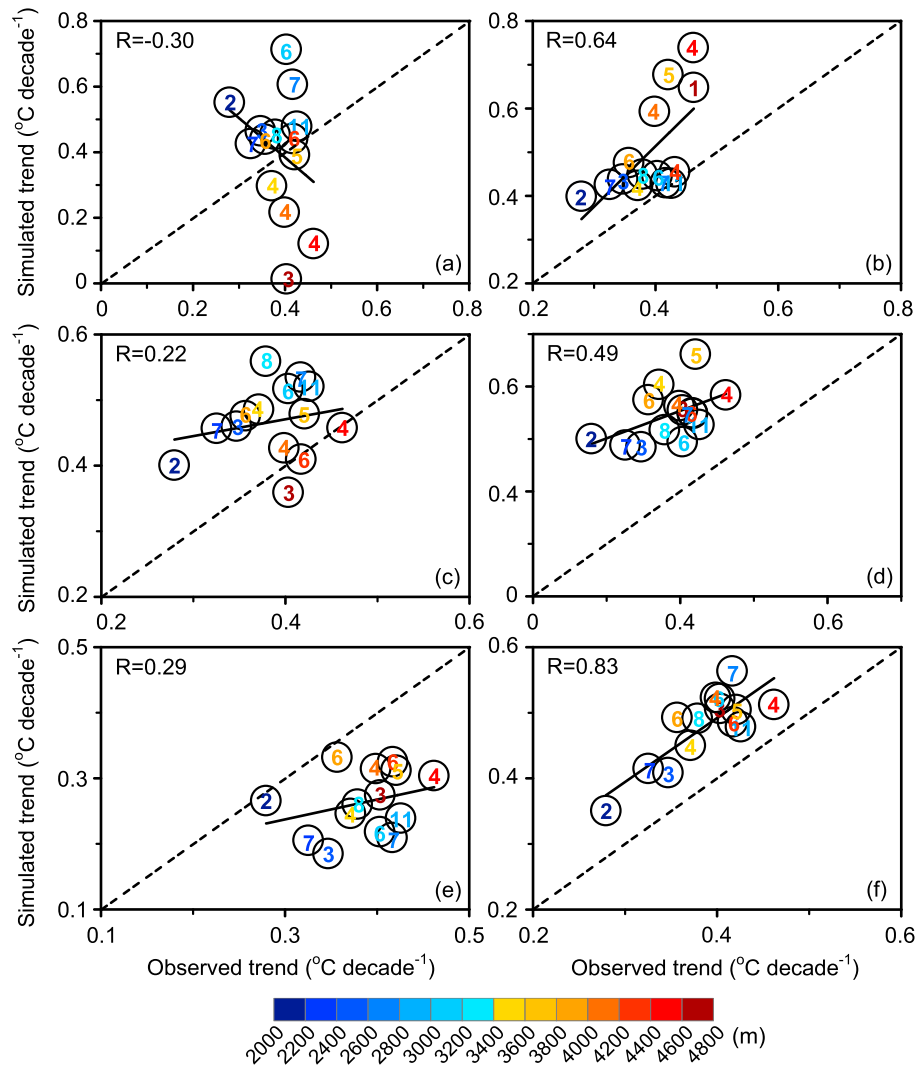


**Figure 2.** Comparison between simulated gridded temperature trends and corresponding station observations with the individual elevation bin mean from (a) HadGEM2-AO/HadGEM3-RA, (b) MIROC5/WRF, (c) HadGEM2-AO/MM5, (d) HadGEM2-AO/WRF, (e) BCC-CSM1.1/RegCM4, and (f) HadGEM2-AO/RegCM4 for the period from 1979 to 2005. The number in each circle represents the number of stations in each elevation bin. *R* denotes the correlation coefficient between the simulated and observed values.

### 3.2. Elevation-Dependent Warming in the Future

As shown in Figure 3a, the warming rates from the HadGEM2-AO/RegCM4 simulation first increase as the elevation increases from 2000 m to 4400 m and then declines as the elevation continues to raise from 4400 to 5600 under the RCP4.5 scenario. The elevation at which the warming rates reach the peak is 4200–4400 m. Similar change characteristics in warming rates can be found under the RCP8.5 scenario (Figure 3b). However, the elevation at which the warming rate reaches the peak increases to a height of 4400–4600 m, which indicates that the elevation-dependent warming law can expand to higher elevation when encountering more serious warming from a higher greenhouse gas emission scenario.

For the MIROC5/WRF simulation, similarly, the warming rates first increase and then decrease along with increasing elevation for both periods from 2006 to 2050 and from 2006 to 2099 under the RCP6.0 scenario (Figures 4a and 4b). The elevations at which the warming rates reach the peak are 4600–4800 m and 5000–5200 m for the period from 2006 to 2050 and from 2006 to 2099, respectively, which also indicates an expansion of the elevation-dependent warming law to higher elevations when continuously more serious warming occurs.

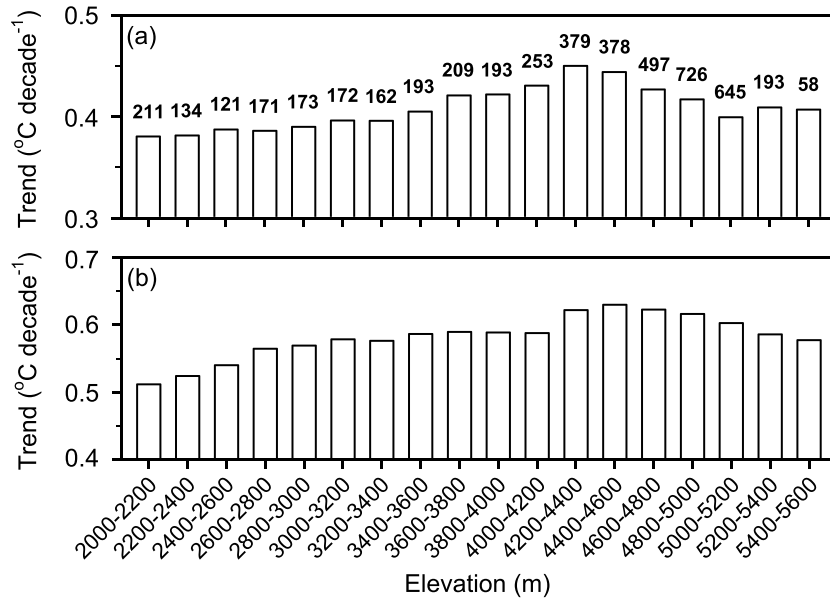


**Figure 3.** Temperature trend change along with increasing elevation for (a) HadGEM2-AO/RegCM4 from 2006 to 2050 under the RCP4.5 scenario and (b) HadGEM2-AO/RegCM4 from 2006 to 2050 under the RCP8.5 scenario. The trends are the means over individual elevation bins. The number above each bar is the number of simulation grids in each elevation bin.

Using the nighttime MODIS land surface temperature, *Qin et al.* [2009] found that the warming rate first increases along with elevation increasing from 3000 to 5200 m and then declines from 5200 m to 5600 m during the period from 2000 to 2006. The future characteristics regarding elevation-dependent warming from the present study are consistent with their current situations, which may suggest that the future estimates are reasonable to some extent.

This study shows that elevation-dependent warming does not expand to 4800 m, except for the case of MIROC5/WRF (2006–2099; RCP6.0). It could not affect most of the glaciers and snow surfaces that are located

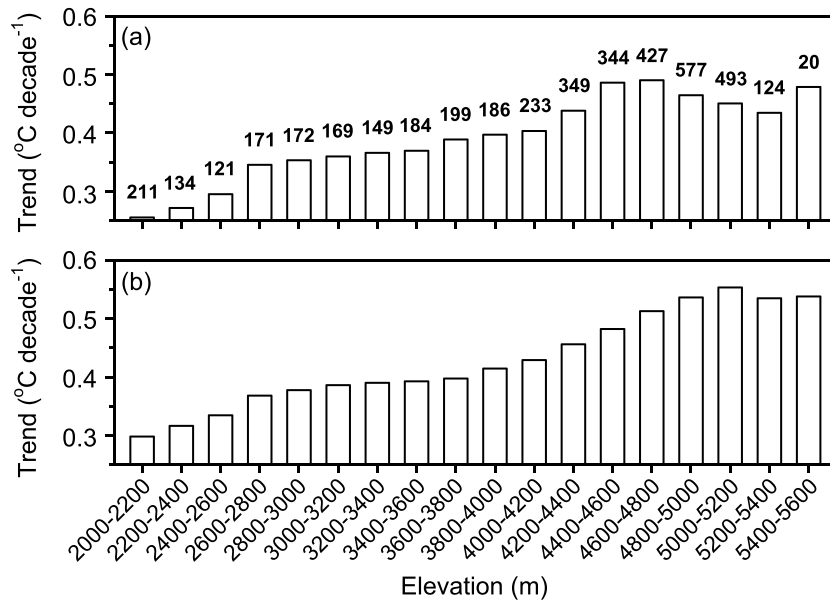


**Figure 4.** Temperature trend change along with increasing elevation for (a) MIROC5/WRF from 2006 to 2050 and (b) MIROC5/WRF from 2006 to 2099 under the RCP6.0 scenario. The trends are the means over individual elevation bins. The number above each bar is the number of simulation grids in each elevation bin.

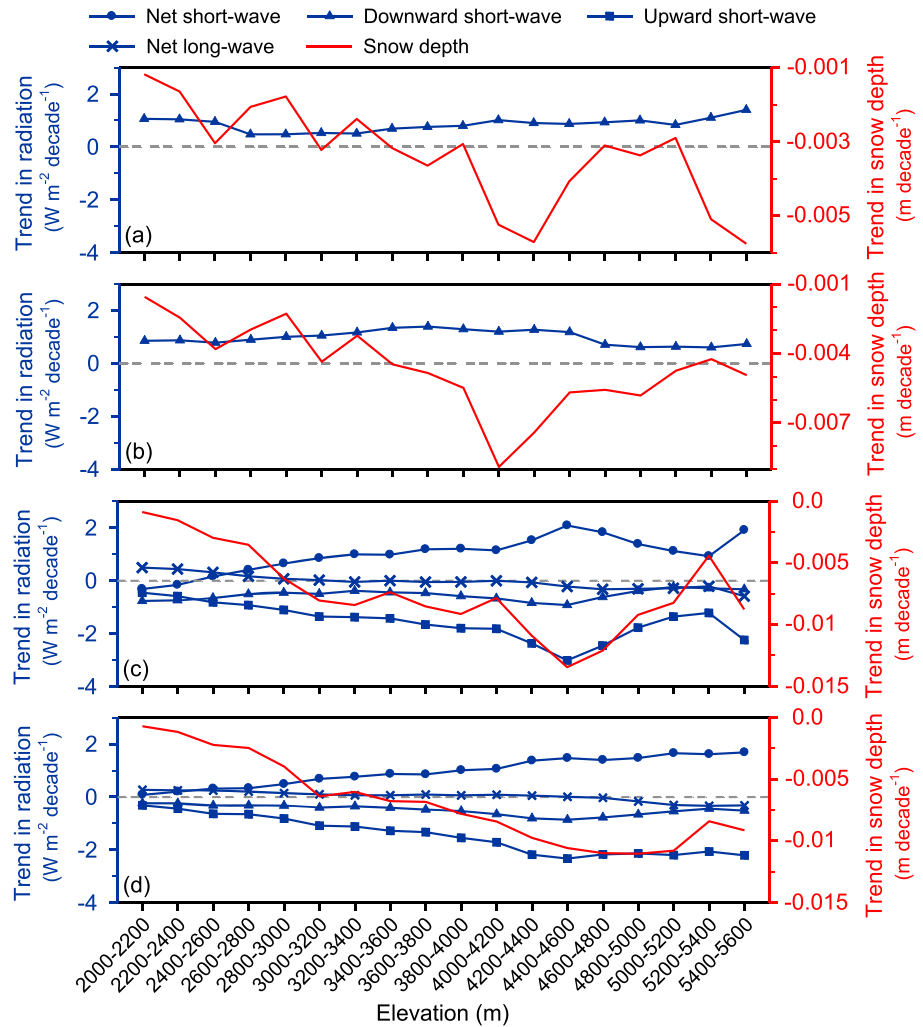


**Figure 5.** Radiation fluxes and snow depth trend changes along with increasing elevation for (a) HadGEM2-AO/RegCM4 from 2006 to 2050 under the RCP4.5 scenario, (b) HadGEM2-AO/RegCM4 from 2006 to 2050 under the RCP8.5 scenario, (c) MIROC5/WRF from 2006 to 2050 under the RCP6.0 scenario, and (d) MIROC5/WRF from 2006 to 2099 under the RCP6.0 scenario. All trends are the means over individual elevation bins. Net short-wave radiation, net long-wave radiation, and upward short-wave radiation are not shown in Figures 5a and 5b due to the lack of data.

in the areas with elevation above 4800 m. However, the warming rate has already increased with a high level at 4800 m, which could still result in the ablation of those solid water reserves. In addition, this study shows that elevation-dependent warming can expand to higher elevations when more serious warming occurs. Thus, large implications for those solid water reserves are expected to be caused by elevation-dependent warming if the warming further intensifies.

### 3.3. Analysis of the Mechanisms

Pepin *et al.* [2015] suggested that a detailed analysis of regional energy budgets is a feasible way to potentially determine the mechanisms for elevation-dependent warming. As shown in Figure 5, among surface net radiation budget, net short-wave radiation appears to be dominant in terms of amount and variation pattern against the distinctly weak net long-wave radiation (Figures 5c and 5d). This indicates that net short-wave radiation is most responsible for elevation-dependent warming. Among the net short-wave radiation budget, upward short-wave radiation appears to be dominant in terms of the amount and variation pattern compared to the distinctly weak downward short-wave radiation (Figures 5a–5d). In addition, upward short-wave radiation variations have a statistically significant correlation with snow, with correlation coefficients of 0.94 and 0.97 for the MIROC5/WRF (2006–2050; RCP6.0) and MIROC5/WRF (2006–2099; RCP6.0)

**Table 2.** Correlation Coefficients Between the Radiation Fluxes and Snow Depth and Air Temperature Trend Changes Along with Increasing Elevation for HadGEM2-AO/RegCM4 from 2006 to 2050 Under the RCP4.5 Scenario, HadGEM2-AO/RegCM4 from 2006 to 2050 Under the RCP8.5 Scenario, MIROC5/WRF from 2006 to 2050 Under the RCP6.0 Scenario, and MIROC5/WRF from 2006 to 2099 Under the RCP6.0 Scenario<sup>a</sup>

Model Name	Net Short-Wave Radiation	Net Long-Wave Radiation	Downward Short-Wave Radiation	Upward Short-Wave Radiation	Snow Depth
HadGEM2-AO/RegCM4 (2006–2050, RCP4.5)			0.20		–0.72 <sup>b</sup>
HadGEM2-AO/RegCM4 (2006–205, RCP8.5)			0.15		–0.72
MIROC5/WRF (2006–2050, RCP6.0)	<b>0.95</b>	–0.95	0.22	–0.87	–0.85
MIROC5/WRF (2006–2099, RCP6.0)	<b>0.97</b>	–0.94	–0.69	–0.87	–0.91

<sup>a</sup>All trends are the means over individual elevation bins.

<sup>b</sup>Bold type represents a statistical significance >95%.

simulations, respectively (Figures 5c and 5d). This correlation indicates that snow variation is mostly responsible for the net short-wave radiation budget. The correlation coefficients between the snow and air temperature trend changes along with increasing elevation are –0.72, –0.72, –0.85, and –0.91 for the HadGEM2-AO/RegCM4 (2006–2050; RCP4.5), HadGEM2-AO/RegCM4 (2006–2050; RCP8.5), MIROC5/WRF (2006–2050; RCP6.0), and MIROC5/WRF (2006–2099; RCP6.0) simulations, respectively, all with statistically significant levels above 95% (Table 1). These analyses indicate that snow-albedo feedback is most responsible for elevation-dependent warming in the future. Previous studies suggested that increase in surface water vapor was responsible for the elevation-dependent warming by increasing downward long-wave radiation [Rangwala *et al.*, 2010]. This study shows that net long-wave radiation is weak, meaning that long-wave radiation has relatively small contributions to the elevation-dependent warming (Table 2).

The elevation-dependent warming is absent when the elevation reaches a certain height (e.g., 4600–4800 m for MIROC5/WRF from 2006 to 2050), which is closely related to snow changes with elevation. Because the present-day (1986–2005) mean air temperatures are much lower than the freezing point when elevations are higher than that height (not shown), the elevation-dependent warming cannot increase them to approach the freezing point and further melt the snow. When snow loss is relatively low, there is a decrease in the warming. This explanation is consistent with the aforementioned phenomenon that elevation-dependent warming tends to expand to higher elevation when more serious warming occurs because the more serious warming has greater chances to increase the present-day mean air temperature state to approach the freezing point. Some other interpretations may also be reasons for the absence of elevation-dependent warming. For example, Yang *et al.* [2014] mentioned that the Tibetan Plateau land surfaces at the higher elevation protrude into the middle-high troposphere; thus, warming at these land surfaces is affected by the midtroposphere’s warming situation, which decreases with respect to increasing elevation.

#### 4. Concluding Remarks

Statistically and dynamically downscaling model simulations could be useful to identify and quantify the historical and future elevation-dependent warming and its causes [Pepin *et al.*, 2015]. This study used data sets from multiple dynamically downscaling simulations to investigate the future elevation-dependent warming and the mechanisms. The validation shows that only two out of six simulations have statistically significant correlations with station observations, indicating that caution is needed when using model simulations to study elevation-dependent warming on the Tibetan Plateau.

Elevation-dependent warming is present at relatively low-elevation ranges but absent when the elevation continues to rise. The watershed with respect to elevation is variable and increases when climate warming intensifies. Energy budget-based analysis shows that snow-albedo feedback is mostly responsible for elevation-dependent warming on the Tibetan Plateau in the future.

Although elevation-dependent warming is absent at high elevation (above 4400–5200 m in this study), which means that there is less impact on most glaciers and snowpack located at elevations above 4800 m, more attention is needed due to the large warming rate that has been increased by elevation-dependent warming in the low-elevation range, as well as the raising watershed with respect to elevation when climate warming intensifies.

The elevation-dependent warming has important implications for solid water reserves on the Tibetan Plateau, which thus has been studied based on meteorological station observations [Liu and Chen, 2000;

Yan and Liu, 2014], satellite remote sensing data [Qin et al., 2009], and numerical simulation method [Liu et al., 2009; Rangwala et al., 2010; Yan et al., 2016]. The major mechanisms are related to snow depletion [Liu et al., 2009; Rangwala et al., 2010; Yan et al., 2016], increase in surface water vapor [Rangwala et al., 2010], and decrease in total cloud [Liu et al., 2009; Yan et al., 2016]. Using the data from the annual 1% CO<sub>2</sub> increase experiment for 100 simulation years by Community Climate System Model version 3 (CCSM3), Liu et al. [2009] found that the increase in downward short-wave radiation (influenced by decrease in total cloud amount) and the decrease in upward short-wave radiation (influenced by decrease in snow depth) were responsible for the elevation-dependent warming. Using the output from GISS-AOM model, Rangwala et al. [2010] showed that the increase in downward long-wave radiation (influenced by increase in surface specific humidity) and the decrease in upward short-wave radiation (influenced by decrease in snow depth) appeared to affect the elevation-dependent warming from 1960 to 2100. Recently, based on the data from the 1990 control and 4 × CO<sub>2</sub> runs by CCSM3 with horizontal resolutions of 1.4° and 3.75°, Yan et al. [2016] showed that the increase in surface net radiation (influenced by the combined effects of decreases in total cloud and snow depth) resulted in elevation-dependent warming on the Tibetan Plateau. This study investigated the future situation of elevation-dependent warming on the Tibetan Plateau using six data sets from dynamical downscaling simulation. A validation of models was taken into account. The results show that decrease in upward short-wave radiation (influenced by decrease in snow depth) is the most responsible for elevation-dependent warming in the future, a conclusion that is supported by significant elevation-based change in upward short-wave radiation but distinctly weak elevation-based change in downward short-wave radiation and net long-wave radiation. For continued study, we can concentrate on investigating and quantifying the historical situation regarding elevation-dependent warming and the associated mechanisms using the multiple dynamical downscaling simulation ensemble and performing sensitivity experiments.

#### Acknowledgments

This research was jointly supported by the CAS-PKU Pioneer Cooperation Program under grant 7-159179, the National Natural Science Foundation of China under grants 41130103 and 41275110, and the Open Research Fund Program of Plateau Atmosphere and Environment Key Laboratory of Sichuan Province under grant PAEKL-2016-K2. Thanks are due to the Coordinated Regional Climate Downscaling Experiment (CORDEX) in East Asia, which provided the partial high-resolution simulation data (<https://cordex-ea.climete.go.kr/main/mainPage.do>), and the China Meteorological Administration, which provided near-surface air temperature data from meteorological station observations. We are indebted to two reviewers for their constructive comments for the initial draft of this paper.

#### References

- Baek, H. J., et al. (2013), Climate change in the 21st century simulated by HadGEM2-AO under representative concentration pathways, *Asia-Pac. J. Atmos. Sci.*, *49*, 603–618.
- Collins, W., P. Rasch, B. Boville, J. Hack, J. McCaa, D. Williamson, J. Kiehl, B. Briegleb, C. Bitz, and S. Lin (2004), Description of the NCAR Community Atmosphere Model (CAM 3.0), *NCAR Tech. Note NCAR/TN-464+STR*.
- Easterling, D., and T. Peterson (1995), A new method for detecting undocumented discontinuities in climatological time series, *Int. J. Climatol.*, *15*, 369–377.
- Gao, X. J., M. L. Wang, and F. Giorgi (2013), Climate change over China in the 21st century as simulated by BCC\_CSM1.1-RegCM4.0, *Atmos. Oceanic Sci. Lett.*, *6*, 381–386.
- Giorgi, F., C. Jones, and G. R. Asrar (2009), Addressing climate information needs at the regional level: The CORDEX framework, *WMO Bull.*, *58*, 175–183.
- Giorgi, F., et al. (2012), RegCM4: Model description and preliminary test over multi CORDEX domain, *Clim. Res.*, *52*, 7–29.
- Guo, D. L., and H. J. Wang (2012), The significant climate warming in the northern Tibetan Plateau and its possible causes, *Int. J. Climatol.*, *32*, 1775–1781.
- Guo, D. L., and H. J. Wang (2013), Simulation of permafrost and seasonally frozen ground conditions on the Tibetan Plateau, 1981–2010, *J. Geophys. Res. Atmos.*, *118*, 5216–5230, doi:10.1002/jgrd.50457.
- Guo, D. L., and H. J. Wang (2014), Simulated change in the near-surface soil freeze/thaw cycle on the Tibetan Plateau from 1981 to 2010, *Chin. Sci. Bull.*, *59*, 2439–2448.
- Guo, D. L., and H. J. Wang (2016), Comparison of a very-fine-resolution GCM and RCM dynamical downscaling in simulating climate in China, *Adv. Atmos. Sci.*, *33*, 559–570.
- Guo, D. L., H. J. Wang, and D. Li (2012), A projection of permafrost degradation on the Tibetan Plateau during the 21st century, *J. Geophys. Res.*, *117*, D05106, doi:10.1029/2011JD016545.
- Han, Z., X. Gao, Y. Shi, J. Wu, M. Wang, and F. Giorgi (2015), Development of Chinese high resolution land cover data for the RegCM4/CLM and its impact on regional climate simulation [in Chinese], *J. Glaciol. Geocryol.*, *37*, 857–866.
- Hong, S. Y., and J. Lim (2006), The WRF single-moment 6-class microphysics scheme (WSM6), *J. Korean Meteorol. Soc.*, *42*, 129–151.
- Hong, S. Y., Y. Noh, and J. Dudhia (2006), A new vertical diffusion package with an explicit treatment of entrainment processes, *Mon. Weather Rev.*, *134*, 2318–2341.
- Hu, Q., D. B. Jiang, and G. Z. Fan (2015), Climate change projection on the Tibetan Plateau: Results of CMIP5 models [in Chinese], *Chin. J. Atmos. Sci.*, *39*, 260–270.
- Immerzeel, W. W., L. P. H. Van Beek, and M. F. P. Bierkens (2010), Climate change will affect the Asian water towers, *Science*, *328*, 1382–1385.
- IPCC (2013), Summary for policymakers, in *Climate Change 2013: The Physical Science Basis. Contribution of Working Group I to the Fifth Assessment Report of the Intergovernmental Panel on Climate Change*, edited by T. F. Stocker et al., pp. 3–29, Cambridge Univ. Press, Cambridge, U. K.
- Ji, Z., and S. Kang (2013), Projection of snow cover changes over China under RCP scenarios, *Clim. Dyn.*, *41*, 589–600.
- Kain, J. S. (2004), The Kain-Fritsch convective parameterization: An update, *J. Appl. Meteorol.*, *43*, 170–181.
- Lawrence, D. M., A. G. Slater, and S. C. Swenson (2012), Simulation of present-day and future permafrost and seasonally frozen ground conditions in CCSM4, *J. Clim.*, *25*, 2207–2225.
- Lee, D. K., D. H. Cha, and H. S. Kang (2004), Regional climate simulation of the 1998 summer flood over East Asia, *J. Meteorol. Soc. Jpn.*, *82*, 1735–1753.
- Li, Q., X. Liu, H. Zhang, T. Peterson, and D. Easterling (2004), Detecting and adjusting on the temporal inhomogeneity in Chinese mean surface air temperature dataset, *Adv. Atmos. Sci.*, *21*, 260–268.

- Li, S., and G. Cheng (1996), *Map of Permafrost Distribution on the Qinghai-Xizang (Tibetan) Plateau, Scale 1:3,000,000* [in Chinese], Gansu Cultural Press, Lanzhou, China.
- Li, X., G. Cheng, H. Jin, E. Kang, T. Che, R. Jin, L. Wu, Z. Nan, J. Wang, and Y. Shen (2008), Cryospheric change in China, *Global Planet. Change*, *62*, 210–218.
- Li, Z., and Z. Yan (2009), Homogenized daily mean/maximum/minimum temperature series for China from 1960–2008, *Atmos. Oceanic Sci. Lett.*, *2*, 237–243.
- Liu, X., and B. Chen (2000), Climatic warming in the Tibetan Plateau during recent decades, *Int. J. Climatol.*, *20*, 1729–1742.
- Liu, X., Z. Cheng, L. Yan, and Z. Yin (2009), Elevation dependency of recent and future minimum surface air temperature trends in the Tibetan Plateau and its surroundings, *Global Planet. Change*, *68*, 164–174.
- Martin, G. M., M. A. Ringer, V. D. Pope, A. Jones, C. Dearden, and T. J. Hinton (2006), The physical properties of the atmosphere in the new Hadley Centre Global Environmental Model (HadGEM1). Part I: Model description and global climatology, *J. Clim.*, *19*, 1274–1302.
- Niu, G., et al. (2011), The community Noah land surface model with multiparameterization options (Noah-MP): 1. Model description and evaluation with local-scale measurements, *J. Geophys. Res.*, *116*, D12109, doi:10.1029/2010JD015139.
- Pepin, N., et al. (2015), Elevation-dependent warming in mountain regions of the world, *Nat. Clim. Change*, *5*, 424–430.
- Qin, D. H., B. T. Zhou, and C. D. Xiao (2014), Progress in studies of cryospheric changes and their impacts on climate of China, *J. Meteorol. Res.*, *28*, 732–746.
- Qin, J., K. Yang, S. Liang, and X. Guo (2009), The altitudinal dependence of recent rapid warming over the Tibetan Plateau, *Clim. Change*, *97*, 321–327.
- Qiu, J. (2008), The third pole, *Nature*, *454*, 393–396.
- Qu, P., M. X. Yang, D. L. Guo, and C. Chen (2009), Simulation of summer air temperature and precipitation over Tibetan Plateau with regional climate model (RegCM3) [in Chinese], *Plateau Meteorol.*, *28*, 738–744.
- Rangwala, I., and J. R. Miller (2012), Climate change in mountains: A review of elevation-dependent warming and its possible causes, *Clim. Change*, *114*, 527–547.
- Rangwala, I., J. Miller, G. Russell, and M. Xu (2010), Using a global climate model to evaluate the influences of water vapor, snow cover and atmospheric aerosol on warming in the Tibetan Plateau during the twenty-first century, *Clim. Dyn.*, *34*, 859–872.
- Rangwala, I., E. Sinsky, and J. R. Miller (2013), Amplified warming projections for high altitude regions of the northern hemisphere mid-latitudes from CMIP5 models, *Environ. Res. Lett.*, *8*, 024040.
- Skamarock, W. C., J. B. Klemp, J. Dudhia, D. O. Gill, D. M. Barker, M. G. Duda, X. Y. Huang, W. Wang, and J. G. Powers (2008), A description of the advanced research WRF version 3, NCAR technical note.
- Su, F., X. Duan, D. Chen, Z. Hao, and L. Cuo (2013), Evaluation of the global climate models in the CMIP5 over the Tibetan Plateau, *J. Clim.*, *26*, 3187–3208.
- Wang, H. J., and J. Q. Sun (2009), Variability of northeast China river break-up date, *Adv. Atmos. Sci.*, *26*, 701–706.
- Wang, H. J., J. Q. Sun, H. P. Chen, Y. L. Zhu, Y. Zhang, D. B. Jiang, X. M. Lang, K. Fan, E. T. Yu, and S. Yang (2012), Extreme climate in China: Facts, simulation and projection, *Meteorol. Z.*, *21*, 279–304.
- Watanabe, M., et al. (2010), Improved climate simulation by MIROC5: Mean states, variability, and climate sensitivity, *J. Clim.*, *23*, 6312–6335.
- Wu, J., X. J. Gao, Y. L. Xu, and J. Pan (2015), Regional climate change and uncertainty analysis based on four regional climate model simulations over China, *Atmos. Oceanic Sci. Lett.*, *8*, 147–152.
- Wu, T., R. Yu, F. Zhang, Z. Wang, M. Dong, L. Wang, X. Jin, D. Chen, and L. Li (2010), The Beijing Climate Center atmospheric general circulation model: Description and its performance for the present-day climate, *Clim. Dyn.*, *34*, 123–147.
- Yan, L., and X. Liu (2014), Has climatic warming over the Tibetan Plateau paused or continued in recent years, *J. Earth Ocean Atmos. Sci.*, *1*, 13–28.
- Yan, L., Z. Liu, G. Chen, J. E. Kutzbach, and X. Liu (2016), Mechanisms of elevation-dependent warming over the Tibetan Plateau in quadrupled CO<sub>2</sub> experiments, *Clim. Change*, doi:10.1007/s10584-016-1599-z.
- Yang, K., H. Wu, J. Qin, C. Lin, W. Tang, and Y. Chen (2014), Recent climate changes over the Tibetan Plateau and their impacts on energy and water cycle: A review, *Global Planet. Change*, *112*, 79–91.
- Yang, M. X., F. Nelson, N. Shiklomanov, D. L. Guo, and G. Wan (2010), Permafrost degradation and its environmental effects on the Tibetan Plateau: A review of recent research, *Earth Sci. Rev.*, *103*, 31–44.
- Yao, T. D., et al. (2012), Third Pole Environment (TPE), *Environ. Dev.*, *3*, 52–64.
- You, Q., S. Kang, E. Aguilar, and Y. Yan (2008), Changes in daily climate extremes in the eastern and central Tibetan Plateau during 1961–2005, *J. Geophys. Res.*, *113*, D07101, doi:10.1029/2007JD009389.
- Yu, E. T., and W. L. Xiang (2015), Projected climate change in the northwestern arid regions of China: An ensemble of regional climate model simulations, *Atmos. Oceanic Sci. Lett.*, *8*, 134–142.
- Yu, E. T., J. Q. Sun, H. Chen, and W. Xiang (2014), Evaluation of a high-resolution historical simulation over China: Climatology and extremes, *Clim. Dyn.*, *45*, 2013–2031.
- Zhang, R. H., F. G. Su, Z. H. Jiang, X. J. Gao, D. L. Guo, J. Ni, Q. L. You, C. Lan, and B. T. Zhou (2015), An overview of projected climate and environmental changes across the Tibetan Plateau in the 21st century [in Chinese], *Chin. Sci. Bull.*, *60*, 3036–3047.
- Zhou, B. T., Q. H. Wen, Y. Xu, L. C. Song, and X. B. Zhang (2014), Projected changes in temperature and precipitation extremes in China by the CMIP5 multi-model ensembles, *J. Clim.*, *27*, 6591–6611.
- Zhou, B. T., Y. Xu, J. Wu, S. Dong, and Y. Shi (2016), Changes in temperature and precipitation extreme indices over China: Analysis of a high-resolution grid dataset, *Int. J. Climatol.*, *36*, 1051–1066.